ACS APPLIED MATERIALS & INTERFACES

Research Article

www.acsami.org

Self-Healable, Tough, and Ultrastretchable Nanocomposite Hydrogels Based on Reversible Polyacrylamide/Montmorillonite Adsorption

Guorong Gao, Gaolai Du, Yuanna Sun, and Jun Fu*

Polymers and Composites Division, Ningbo Institute of Materials Technology and Engineering, Chinese Academy of Sciences, Zhongguan West Road 1219, Zhenhai District, Ningbo 315201, People's Republic of China

Supporting Information

ABSTRACT: Nanocomposite hydrogels with unprecedented stretchability, toughness, and self-healing have been developed by in situ polymerization of acrylamide with the presence of exfoliated montmorillonite (MMT) layers as noncovalent cross-linkers. The exfoliated MMT clay nanoplatelets with high aspect ratios, as confirmed by transmission electron microscopy (TEM) and X-ray diffraction (XRD) results, are well dispersed in the polyacrylamide matrix. Strong polymer/MMT interaction was confirmed by Fourier transform infrared spectroscopy (FTIR) and differential scanning calorimetry (DSC). The effective cross-link densities of these hydrogels are estimated in the range of 2.2−5.7 mol m^{-3}. Uniaxial tensile tests showed a very high fracture elongation up to 11 800% and a fracture toughness up to 10.1 MJ m^{-3}. Cyclic loading−unloading tests showed remarkable hysteresis, which indicates energy dissipation upon deformation. Residual strain after cyclic loadings could be recovered under mild conditions, with the recovery extent depending on clay content. A mechanism based on reversible desorption/adsorption of polymer chains on clay platelets surface is discussed. Finally, these nanocomposite hydrogels are demonstrated to fully heal by dry−reswell treatments.

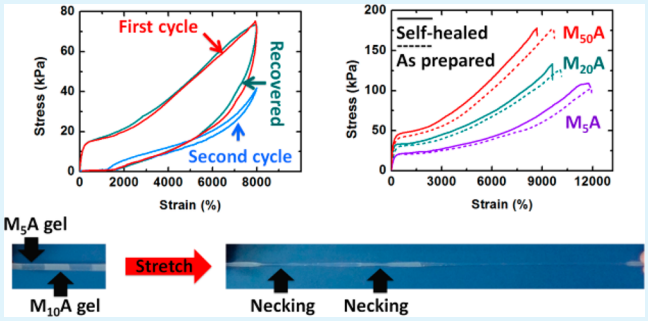

KEYWORDS: *nanocomposite hydrogels, tough, stretchable, self-heal, montmorillonite*

INTRODUCTION

Tissues or organs in living organisms, in response to damage, are generally repaired automatically or externally assisted to regenerate their original structures and functions. Inspired by biological systems, self-healable hydrogels have been drawing extensive research enthusiasm and efforts. Reversible interactions, including hydrogen bonding,[1−3] hydrophobic interactions,[4,5] host−guest recognition,[6−8] or electrostatic interactions,[9] etc., have been widely exploited to create self-healing hydrogels. Most self-healing hydrogels based on noncovalent interactions, however, possess poor mechanical strength and toughness, which limits their applications. It remains a great challenge to create self-healing hydrogels with excellent strength, toughness, and recoverability.

Multiple mechanisms including noncovalent interactions have been used as sacrificial bonds to synthesize tough and stretchable hydrogels.[9−14] Hydrogels based on reversible sacrificial bonds could recover under properly controlled stimulus after unloading.[9,11] For example, alginate/polyacrylamide (PAAm) hybrid hydrogels[11] based on Ca^{2+}-cross-linking show high strength and stretchability (∼2300%), and recover to the original tensile properties after restoration.

Haraguchi pioneered nanocomposite (NC) hydrogels through in situ free radical polymerization of monomers (e.g., *N*-isopropylacrylamide (NIPAAm),[15,16] *N*,*N*′-dimethylacrylamide (DMAA),[17] or acrylamide) with the presence of synthetic clay. For example, PNIPAAm/Laponite XLG hydrogels exhibited a fracture strain (ε_b) up to 1000% and fracture strength (σ_b) of 1.1 MPa.[18] In another case, PAAm/Laponite RDS hydrogels showed a ε_b of 4070% and σ_b of 107 kPa.[19] By using graphene oxide (GO) as multifunctional cross-linkers, PAAm/GO hydrogels showed a ε_b up to 3525% and σ_b around 300 kPa.[20] Most recently, layered double hydroxide (LDH) nanosheets have been reported to serve as two-dimensional inorganic cross-linkers to generate PAAm/LDH hydrogels with very high extensibility (∼6000%) but low strength (∼30−50 kPa).[21]

So far, only a few strong and tough noncovalent hydrogels have been reported to self-heal. Nanocomposite hydrogels could self-heal through chain migration across damaged interface and readsorption to neighboring clay surfaces.[22] The mechanical properties could fully recover to those of as-prepared hydrogels. Moreover, nanocomposite hydrogels composed of graphene peroxide (GPO) nanosheets with much larger lateral dimensions

Received: January 23, 2015
Accepted: February 10, 2015
Published: February 10, 2015

DOI: 10.1021/acsami.5b00704
ACS Appl. Mater. Interfaces 2015, 7, 5029−5037

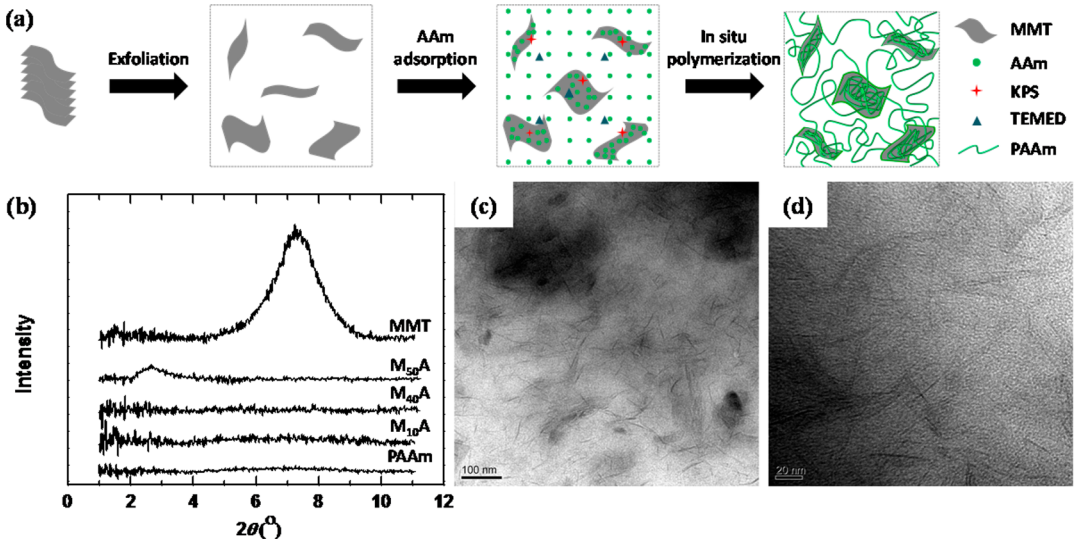

Figure 1. (a) Schematic illustration of the synthesis of M_nA hydrogels. (b) XRD profiles of original MMT, M_nA hydrogels with different MMT contents, and neat PAAm. (c, d) Representative TEM images of the $M_{50}A$ hydrogel.

are able to self-heal and show high stretchability (~5000%) and σ_b of 340 kPa.[23] Amphiphilic copolymer hydrogels based on hydrophobic associations exhibited capability to self-heal, and showed a ε_b of 3600 ± 630% with a relatively low strength of 12 ± 1 kPa.[4] The scarcity of strong, tough, and self-healable hydrogels seriously limits the research on such materials and their applications. More efforts are needed to enrich current understanding of toughening and self-healing in order to boost the development of novel tough and healable hydrogels that meet demands from industrial or biomedical applications.

In this work, we use exfoliated sodium montmorillonite (NaMMT) as noncovalent cross-linkers for a novel synthesis of tough hydrogels. NaMMT is a layered silicate clay constituted by two tetrahedral silica sheets sandwiching an octahedral sheet formed from cations such as Al^{3+} or Mg^{2+}, with a formula of $[(Al,Mg)_4Si_8O_{20}(OH)_4]Na_{0.66}$ (different from Laponite XLG, $[Mg_{5.34}Li_{0.66}Si_8O_{20}(OH)_4]Na_{0.66}$). Exfoliated montmorillonite (MMT) nanosheets are about 1 nm thick and extend to 100–1000 nm in two dimensions,[24] with an aspect ratio larger than that of Laponite XLG (around 30 nm diameter × 1 nm thickness). It is well-known that montmorillonite (MMT) is able to adsorb organic molecule on the surface,[25−30] and has been applied in polymer nanocomposites,[24,31] superabsorbents,[32] and drug-releasing materials.[33] MMT has also been used to reinforce chemically cross-linked polymer hydrogels, showing limited enhancement in strength and toughness due to the intrinsically inhomogeneous chemical networks.[34] To the best of our knowledge, MMT has never been used as multifunctional cross-linkers to synthesize tough, stretchable, and self-healing hydrogels without using any chemical cross-linkers.

Herein, we used exfoliated NaMMT nanosheets for in situ polymerization of acrylamide monomers, resulting in nanocomposite hydrogels with clay contents up to 50 wt % with respect to polymers. Upon tensile tests, these hydrogels showed typical yielding, necking, and strain hardening, as well as a fracture elongation up to 11 800% and a fracture toughness up to 10.1 MJ m^{-3}. The polymer–clay interaction mechanism has been systematically investigated by cyclic loading–unloading tensile tests with designed stretching protocols. Moreover, tensile tested hydrogels are demonstrated to recover under mild conditions through reversible readsorption of polymer chains to clay surfaces. Finally, these hydrogels are demonstrated to self-heal through a controlled dry–swell process.

EXPERIMENTAL SECTION

Materials. Acrylamide (AAm), *N*,*N*′-methylene-bis(acrylamide) (MBAA), potassium persulfate (KPS), and *N*,*N*,*N*′,*N*′-tetramethylethylenediamine (TEMED) were purchased from the Sinopharm Chemical Reagent Co., Ltd. and used as received. Sodium montmorillonite (Na-MMT) was kindly supplied by Zhejiang Fenghong New Material Co., Ltd. and used after washing and freeze-drying. Milli-Q water (Millipore, USA) was used for all experiments, with oxygen removed by bubbling nitrogen gas for more than 3 h before use.

Hydrogel Synthesis. The PAAm/MMT nanocomposite hydrogels were synthesized by in situ free-radical polymerization of AAm in the presence of exfoliated MMT. Typically, MMT (0.64 g) was dispersed in water (28 mL) under ultrasonication for 1 h. Subsequently, AAm (6.4 g, 90 mmol) was added to the clay suspension, followed by magnetic stirring for 1 day at room temperature. Then initiator KPS (0.1 g) in water (2 mL) and accelerator TEMED (55.5 μL) were injected into the mixture at ice–water temperature. After the solution was mixed for an additional 30 min, the solution was transferred into glass tubes with 5.5 mm inner diameter. Polymerization was carried out in air bath at 20 °C for 48 h. The clay content was varied from 5 to 50 wt % with respect to the AAm weight. For comparison, covalently cross-linked PAAm hydrogel was prepared by using 0.1 mol % MBAA with respect to AAm. Linear PAAm was also synthesized without using any cross-linkers.

Characterizations. The nanocomposite hydrogels were lyophilized and then milled into powders. X-ray diffraction (XRD) patterns of these powders were obtained by using the Cu Kα X-ray beam on a D8 Discover X-ray diffractometer (Bruker, Germany) at 40 kV and 40 mA. The spacing of MMT layers in xerogel is calculated from Bragg's law: $2d\sin\theta = n\lambda$. Where λ is the wavelength of the incident beam, 2θ is the angle between incident and scattered X-ray wavevectors, and n is the interference order.[35]

For transmission electron microscopy (TEM) imaging, lyophilized hydrogels were embedded in epoxy resin for microtoming at −40 °C with a glass knife to ca. 50 nm thick sections, which were collected onto copper grids for imaging in a transmission electron microscope (Tecnai F20, FEI Inc., Oregon) at 200 kV. No contrasting was needed.

Fourier transform infrared (FTIR) spectroscopy of vacuum-dried hydrogel slices were recorded by using a Cary 640 spectrometer (Agilent, Australia) at attenuated total reflectance (ATR) mode. Differential scanning calorimetry (DSC) measurements on vacuum-dried gels were performed by using a Mettler Toledo TGA/DSC 1 system from 25 to 250 °C at 10 °C min^{-1}.

DOI: 10.1021/acsami.5b00704
ACS Appl. Mater. Interfaces 2015, 7, 5029–5037

Table 1. Formulations[a], Swelling and Structure Parameters of M_nA and $MBAA_{0.1}A$ Hydrogels

gels	water (mL)	AAm (g)	MMT (g)	MBAA (mg)	ESR[b]	$\tau_\alpha = 2^c$ (kPa)	N^{*d} (mol m^{-3})
M_5A	30	6.4	0.32		105 ± 10	9.6	2.2
$M_{10}A$	30	6.4	0.64		58 ± 4	11.8	2.7
$M_{20}A$	30	6.4	1.28		18 ± 1	16.4	3.8
$M_{30}A$	30	6.4	1.92		16 ± 2	19.2	4.4
$M_{40}A$	30	6.4	2.56		12 ± 2	23	5.3
$M_{50}A$	30	6.4	3.2		11 ± 1	24.9	5.7
$MBAA_{0.1}A$	30	6.4		13.8	20 ± 2		

[a]For all hydrogel synthesis, the amount of initiator and accelerator were fixed at 0.1 g (KPS) and 55.5 μL (TEMED). [b]Equilibrium swelling ratio. [c]Stress at 100% strain. [d]Effective cross-link density calculated from eq 3.

Swelling Measurements. Freeze-dried hydrogel samples were immersed in a large excess amount of deionized water at 25 °C for 60 h to reach equilibrium, with water replaced every 12 h. The equilibrium swelling ratio (ESR) was calculated as, $ESR = (W_s - W_d)/W_d \times 100\%$, where W_s and W_d are the weights of the swollen hydrogels and the corresponding dried gels.

Tensile Tests. An Instron 5567 testing machine (Instron, MA, USA) equipped with a 500 N load cell was used for tensile testing. As-prepared hydrogel samples ($n = 5$ each) with 5.5 mm diameter, 45 mm length, and 5 mm gauge length were tested at a crosshead speed of 100 mm min^{-1} and at 25 °C. To avoid water evaporation, a thin layer of silicon oil was sprayed on the sample surface. The engineering tensile stress (σ) was calculated as $\sigma = F/\pi R^2$, where F is the load and R is the original radius of the specimen. The engineering tensile strain (ε) was defined as the change in length (l) relative to the initial gauge length (l_0) of the specimen, $\varepsilon = (l - l_0)/l_0 \times 100\%$. The initial modulus ($E$) was calculated as the slope of the stress−strain curve within the range $\varepsilon = 50\% \sim 100\%$. The fracture toughness was characterized by the fracture energy (U, MJ m^{-3}), which is calculated by integrating the area under the stress−strain curve:

$$U = \int \sigma \mathrm{d}\varepsilon \tag{1}$$

Cyclic tensile tests with a maximum strain of 8000% were conducted on specimens with the same gauge length and at the same crosshead speed. Consecutive loading−unloading cycles with a progressive gradual strain increase of 2000% were conducted to samples until 8000% strain. The dissipated energy for each cycle, ΔU, is defined as the area of hysteresis loop encompassed by the loading−unloading curve:

$$\Delta U = \int_{\text{loading}} \sigma \mathrm{d}\varepsilon - \int_{\text{unloading}} \sigma \mathrm{d}\varepsilon \tag{2}$$

Self-Healing. The as-prepared hydrogels were cut into short rods, which were subsequently put together with the fracture surfaces contacting with each other. This assembly was successively dried at 25 °C for 1 day and at 50 °C in an oven for 6 h to reduce the water content to below 10 wt %. Then, the dried hydrogels were immersed in water until reswollen to their original weight. Finally, the reswollen hydrogels were maintained in sealed polyethylene bags for 3 days before testing.

RESULTS AND DISCUSSION

Synthesis and Structures of PAAm/MMT Nanocomposite Hydrogels. The MMT exfoliation and in situ polymerization procedure is depicted in Figure 1a. MMT was pre-exfoliated in water with ultrasonication and further exfoliated by acrylamide (AAm) to form a homogeneous dispersion. Then redox initiator KPS and TEMED were added to initiate in situ free radical polymerization without using any chemical cross-linkers. The obtained hydrogels are referred to as M_nA hydrogels, where n stands for the clay weight percentage with respect to monomer AAm. Chemically cross-linked PAAm hydrogel with 0.1 mol % MBAA is referred as $MBAA_{0.1}A$. Formulations for hydrogel synthesis are summarized in Table 1.

X-ray diffraction (XRD) (Figure 1b) and transmission electron microscopy (TEM) (Figure 1c, d) results demonstrate the exfoliation and excellent dispersion of MMT platelets in PAAm matrix. In Figure 1b, a strong diffraction peak at $2\theta = 7.3°$ of MMT powders corresponding to the layered structure (spacing between clay sheets d = 1.21 nm) disappeared in freeze-dried M_nA hydrogels with different clay contents. Only with very high clay content ($M_{50}A$), a very weak and broad diffraction at about 2.67° indicates a large spacing (d = 3.31 nm) between the clay layers. TEM images of $M_{50}A$ (Figure 1c,d) xerogel provide direct evidence to excellent dispersion of exfoliated clay platelets (dark gray) in the polymer matrix. More TEM images are available in Figure S1 (Supporting Information). Most of the MMT nanosheets are single layers with thickness of about 1 nm (Figure 1d) and lateral dimension of about 100−200 nm. Moreover, it is interesting that many nanoplatelets appeared twisted or folded appearance (Figures 1d and S1, Supporting Information). These structures may increase the desorption energy of PAAm chains at high strain and allow for additional energy dissipation. These XRD and TEM results indicate that the MMT layers have been dramatically exfoliated and well dispersed in the PAAm matrix.

The equilibrium swelling ratio (ESR) values of M_nA hydrogels are listed in Table 1. The ESR decreased with increasing clay content (C_{clay}), suggesting that the cross-link density was increased with increasing MMT content. When $n \geq 20$, the ESR of M_nA hydrogels became less than that of $MBAA_{0.1}A$ hydrogel (Table 1). The M_nA hydrogels did not dissolve in a large excess amount of deionized water at ambient temperature for more than 6 months. These results indicate that the noncovalently cross-linked networks are stable in water. However, these hydrogels were dissolved in 5 mol L^{-1} urea solution and formed a viscous liquid (Figure S2, Supporting Information). Urea is known as an efficient hydrogen bond-breaking reagent.[36,37] This result suggests that the PAAm/MMT nanocomposite hydrogels are primarily based on hydrogen bonding between the PAAm chains and the clay nanosheets.

The formation of hydrogen bonding between hydroxyl groups and amide groups was further confirmed by FTIR (Figure 2a). The band at 3620 cm^{-1} is attributed to the stretching of structural hydroxyl of MMT, and that at 3415 cm^{-1} is related to H_2O adsorbed on MMT.[38] In the M_nA hydrogels, the −OH band from MMT was strongly suppressed. The N−H bands at 3336 and 3191 cm^{-1} in PAAm shifted to 3293 and 3180 cm^{-1} in $M_{50}A$. Meanwhile, the peak at 1608 cm^{-1} of NH_2 bending in PAAm shifts to 1596 cm^{-1} in $M_{50}A$. In contrast, these bands in $MBAA_{0.1}A$ gel are the same as those in PAAm. These results suggest the formation of hydrogen bonding between PAAm and MMT. It is noted that H-bonds also exist between PAAm chains, but have negligible contribution to hydrogel formation. In

DOI: 10.1021/acsami.5b00704
ACS Appl. Mater. Interfaces 2015, 7, 5029−5037

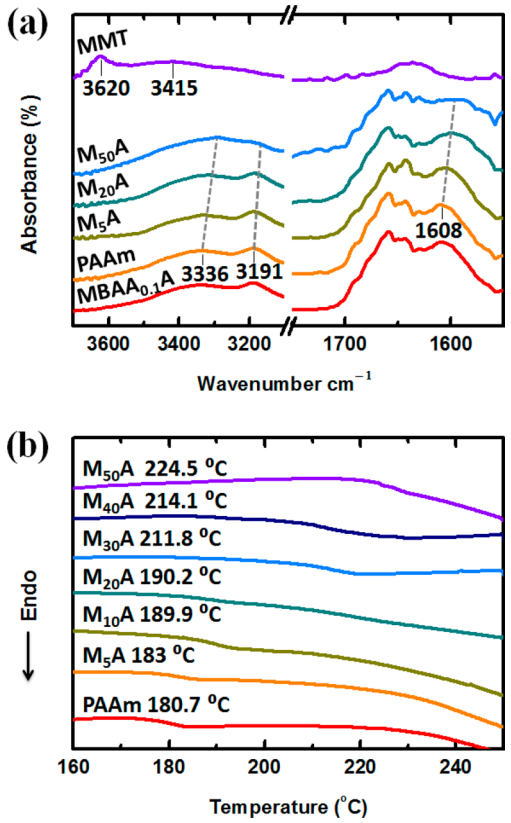

Figure 2. (a) ATR-FTIR spectra of lyophilyzed M_nA hydrogels, $MBAA_{0.1}A$ hydrogel, linear PAAm and MMT powder. (b) Differential scanning calorimetric traces of M_nA hydrogels with different clay contents.

addition, the carbonyl groups of PAAm may complex with the metal ions on clay surface and thus strengthen PAAm/clay association.[39,40]

The strong polymer−clay interaction was further investigated by measuring the glass transition temperature (T_g) of the M_nA hydrogels by DSC. T_g is an indicator to the polymer segment mobility and increases as the chain mobility is hindered.[24] Herein, the T_g of neat linear PAAm is 180.7 °C (Figure 2b), close to the reported value (186.3 °C[41] or 180.8 °C[21]). The T_g of M_nA hydrogels was increased to 183, 189.9, 190.2, and 224.5 °C as the C_{clay} was increased to 5, 10, 20, and 50 wt %. These results provide evidence to the strong interactions of polymer chains to clay surfaces.

Estimation of Cross-Link Density. To approximately evaluate the network structures of these hydogels based on noncovalent interactions, the cross-link densities of M_nA and $MBAA_{0.1}A$ hydrogels were estimated by using the kinetic theory of rubber elasticity[17,19,42]

$$\tau = N^*RT(\alpha - \alpha^{-2}) \quad (3)$$

where τ is the force per unit original area of the stretched hydrogel, N^* is the effective cross-link density, R and T are the gas constant and absolute temperature, and α is the extension ratio. Here $\alpha = 2$ (strain 100%) and $T = 298.15$ K. The τ values at $\alpha = 2$ and calculated N^* values are listed in Table 1. N^* was increased from 2.2 to 5.7 mol m^{-3} as the C_{clay} was increased from 5 to 50 wt %. Meanwhile, the effective cross-link density of chemically cross-linked $MBAA_{0.1}A$ hydrogel is estimated as 3 mol m^{-3}, assuming 100% consumption of MBAA during polymerization. This value is close to those of M_nA hydrogels (Table 1). Therefore, it is reasonable to use the $MBAA_{0.1}A$ hydrogel as a control to the M_nA hydrogels to investigate the role played by the noncovalent cross-linking in the mechanical properties of hydrogels.

It is noted that these estimated cross-link density values are comparable to those of PAAm/Laponite hydrogels by Tong et al.[19] and PAAm/LDH hydrogels by Chen et al.[21] by using the rubbery elasticity theory. Therefore, as to be seen below, the difference of mechanical properties of hydrogels in this study and

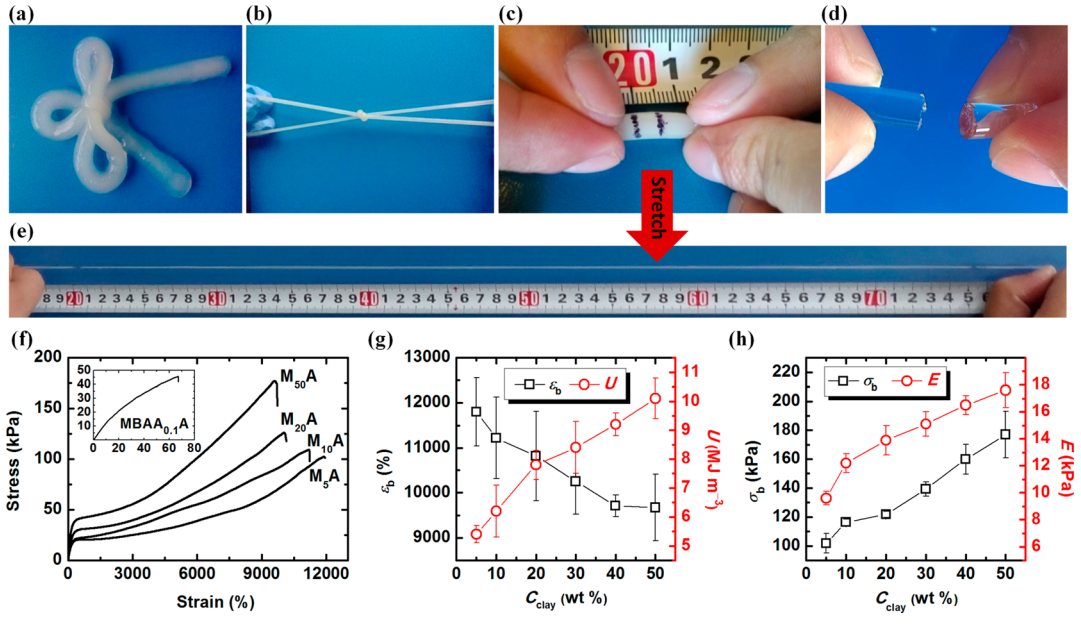

Figure 3. Photographs of a $M_{10}A$ hydrogel bow-tie (a) and that highly stretched (b). Panels c and e show a stretching of the $M_{10}A$ hydrogel to a strain of 11 000%. (d) Covalently cross-linked $MBAA_{0.1}A$ hydrogel shows a brittle fracture at low strain. (f) Representative uniaxial tensile stress−strain curves of M_5A, $M_{10}A$, $M_{20}A$, and $M_{50}A$ hydrogels; inset is that of $MBAA_{0.1}A$ hydrogel. (g) Fracture strain (ε_b) and fracture energy (U) of the M_nA hydrogels as a function of clay content. (h) Fracture stress (σ_b) and initial modulus (E) as a function of clay content.

DOI: 10.1021/acsami.5b00704
ACS Appl. Mater. Interfaces 2015, 7, 5029−5037

those in literature should not be attributed to the cross-link density difference. Instead, the noncovalent interactions between PAAm chains and MMT nanosheets are postulated to primarily account for the outstanding stretchability and toughness of the M_nA hydrogels.

Mechanical Properties of PAAm/MMT Nanocomposite Hydrogels. Despite of the high clay contents, these hydrogels are very soft and flexible, and could be knotted and highly stretched without fracturing at the knot (Figure 3a,b). In fact, the $M_{20}A$ hydrogel, for example, was stretched to 11 000% strain without fracturing (Figure 3c,e), in sharp contrast to the brittle fracture of the chemically cross-linked $MBAA_{0.1}A$ hydrogel (Figure 3d).

The tensile properties of these nanocomposite hydrogels have been systematically investigated. Representative tensile stress−strain ($\sigma-\varepsilon$) curves of the as-prepared M_nA hydrogels are shown in Figure 3f. The tensile strain (ε_b) and fracture energy (U) are summarized in Figure 3g. The σ_b and initial modulus (E) are summarized in Figure 3h. In contrast to the $MBAA_{0.1}A$ gel that fractured at 68% strain and 46 kPa (Figure 3f), the M_nA gels showed extraordinary tensile properties that have never been reported in other strong and tough hydrogels. Two unique and important findings are drawn from these results.

First, all of the M_nA hydrogels yielded at low strain, followed by necking and strain hardening (Figure 3f), which is not seen in $MBAA_{0.1}A$ hydrogel and most other covalently cross-linked hydrogels.[43−45] At low strain, the hydrogels experienced an elastic deformation with a high slope (modulus), which could recover to their original length once unloaded. Yielding occurred at a critical strain, followed by necking, elongation, and strain hardening until the sample broke. The yield strength was enhanced with increasing clay content. Yielding has been well-known for semicrystalline polymers as a result of plastic deformation of spherulites. Recently, yielding and necking have also been reported for double network hydrogels when the rigid first network is fractured,[46] and for poly(2-methoxyethyl acrylate)/Laponite nanocomposites by plastic flow of clay and polymer chains.[47] Such yielding behavior, however, has been rarely reported for nanocomposite hydrogels. Herein, yielding may root from the abrupt detachment of polymer chains from clay surface. This will be demonstrated and discussed below.

Second, these M_nA hydrogels show extraordinary stretchability (Figure 3f). The fracture strain (ε_b) was as high as 11 800% for M_5A. With increasing clay content, the ε_b decreased to ~9600% for $M_{50}A$ (Figure 3f,g). These ε_b values are about 2−10 times higher than other nanocomposite hydrogels based on synthetic clay (Laponite XLG,[18] Laponite XLS,[48] Laponite RDS[19]), layered double hydroxide (LDH),[21] or graphene oxide (GO)[20] nanosheets, and polymers of NIPAAm,[18] DMAA,[17] and AAm[19−21,48] monomers (Figure 4), although the estimated cross-link densities are close to those in literature. However, the σ_b of 100−180 kPa (Figure 3f, h) fell into a medium level among those in literature (Figure 4). The ultra high elongation and high strength resulted in very high fracture energy (U), which is characterized by the area under the stress−strain curve. U was monotonically increased from about 5.4 MJ m^{-3} for M_5A to 10.1 MJ m^{-3} for $M_{50}A$ (Figure 3g). These values are comparable to those for double network hydrogels.[49] The difference in ε_b and σ_b of various hydrogels in Figure 4 may be related to the hydrophobicity of monomers and dimensions of nanoparticles used to prepare the hydrogels. To further improve the tensile strength of these hydrogels, additional noncovalent interactions

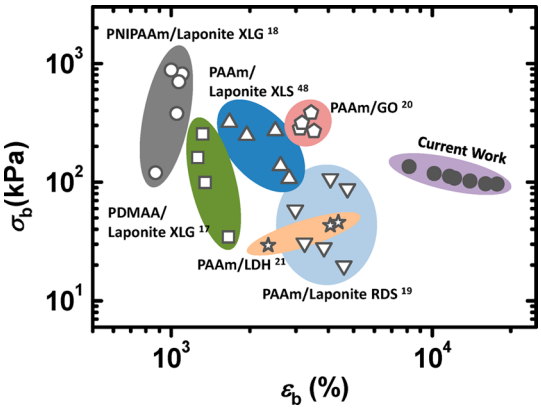

Figure 4. Account of fracture stress (σ_b) and strain (ε_b) of representative nanocomposite hydrogels by in situ polymerization of acrylamides with the presence of synthetic clay or graphene oxide (GO) nanosheets, in comparison to the M_nA hydrogels in this work. Laponite XLG, $[Mg_{5.34}Li_{0.66}Si_8O_{20}(OH)_4]Na_{0.66}$. Laponite XLS, 92.32 wt % $[Mg_{5.34}Li_{0.66}Si_8O_{20}(OH)_4]Na_{0.66}$, 7.68 wt % $Na_4P_2O_7$. Laponite RDS, $[Mg_{5.5}Li_{0.3}Si_8O_{20}(OH)_4]Na_{0.7}$ modified by $Na_4P_2O_7$. LDH, $[Mg_{2.52}Al(OH)_7](HO(CH_2)_2\ SO_3)\cdot 1.27H_2O$.

such as hydrophobic association may be introduced in these nanocomposite hydrogels.

Energy Dissipation and Recovery of PAAm/MMT Nanocomposite Hydrogels. To investigate the yielding and elongation mechanisms, the M_nA hydrogels were subjected to stepwise cyclic tensile loading−unloading tests with consecutive strain increment. This method was used by Gong et al.[50,51] to investigate the internal fracture mechanism of double network (DN) hydrogels. Here, we use this method to investigate the internal structure change of M_nA hydrogels. Upon first loading to 2000% strain, the M_5A hydrogel showed a yield strength (σ_y) of 10.8 kPa. Subsequent unloading left a residual strain of 460%. The sample was immediately loaded to ε_m 4000%. This loading curve before 2000% strain almost overlapped the first unloading curve, followed by yielding at $\varepsilon \approx 2450\%$ with a σ_y of 16.7 kPa, and necking and strain hardening up to 4000% strain. Subsequent loading curves to ε_m of 6000% and 8000% also overlapped the previous unloading curves. Moreover, yielding and strain hardening followed, with σ_y increasing to 29.5 and 34.1 kPa. After unloading from each cycle, the residual strain was increased to 730%, 1000%, and 1500%. Similar yielding, strain hardening, and overlapping of incremental loading−unloading curves are also observed for $M_{10}A$ (Figure 5b) and other M_nA hydrogels (Figure S3, Supporting Information). With higher clay contents, the yield strength and strain hardening modulus for each cycle were higher.

In the M_nA hydrogels, the unexpected yielding phenomenon for each cycle (Figure 5a,b) suggests a hierarchical abrupt desorption of polymer chains from clay surfaces at critical strains. It has been suggested that polymer chains may form diverse attachments on clay surface.[39] The polymer chains may be graded according to the adsorption strength (E_{ad}) to clay and the chain length (l_c) between two adjacent clay platelets. Upon stretching, segments with the shortest l_c and lowest E_{ad} were detached from clay surfaces, resulting in a yield. Subsequent stretching of the detached segments resulted in strain hardening. After unloading, the detached chains could not immediately readsorb onto clay surfaces and thus the second loading appeared rubbery before 2000% strain, with the second stretching curve overlapped the first unloading curve (Figure 5a,b). Further

DOI: 10.1021/acsami.5b00704
ACS Appl. Mater. Interfaces 2015, 7, 5029−5037

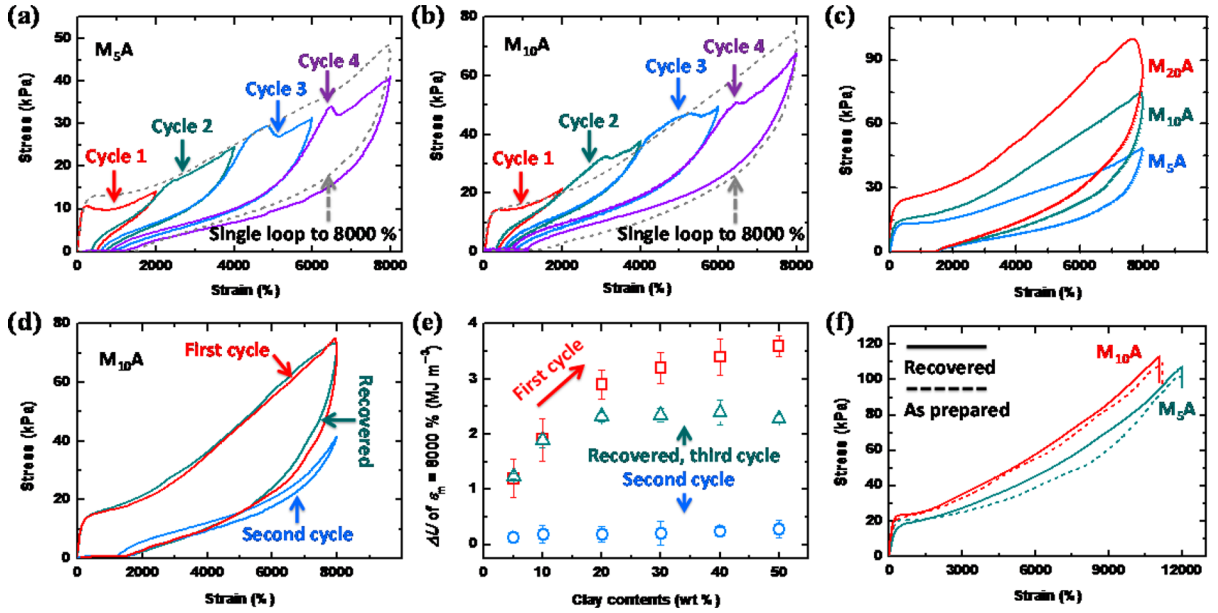

Figure 5. Representative cyclic tensile loading–unloading curves with gradual strain increase up to 8000% strain for the M_5A (a) and $M_{10}A$ (b) hydrogels. The dashed lines are the loading–unloading curves with 8000% strain for the same gels. (c) Tensile loading–unloading curves of M_5A, $M_{10}A$, and $M_{20}A$ hydrogels. (d) Two successive loading–unloading curves of $M_{10}A$ gel and that after recovery at 25 °C for 5 days. (e) Clay content dependence of energy dissipation upon loading–unloading with 8000% strain for the first, immediate second, and third cycles after restoration at 25 °C for 5 days. (f) Representative ultimate tensile stress–strain curves of as-prepared (dashed lines) and recovered (solid lines) M_5A and $M_{10}A$ hydrogels.

loading to strains above 2000% stretched the chains with the second shortest l_c and lowest E_{ad}, which accumulatively detached from the surfaces, resulting in a yield. This procedure repeats during the incremental loading–unloading tests. The strain hardening is related to chain stretching and orientation of clay platelets along with the tensile direction.[52]

The polymer/clay desorption is postulated to dissipate energy and blunt the crack tip as sacrificial bonds, and thus toughen the hydrogels. Tensile loading–unloading tests with 8000% strain were conducted for the M_nA hydrogels with different clay contents. Hysteresis loops are observed for all the M_nA samples (Figure 5c). In contrast, the $MBAA_{0.1}A$ hydrogel showed no energy dissipation loops upon deformation (Figure S4, Supporting Information). The loop area was increased with increasing clay contents (Figure 5c,e). Residual strains of about 1500% were observed after unloading, which suggests that the detached chains did not immediately readsorb to clay surfaces during unloading. This has been confirmed by performing a second loading–unloading test to ε_m = 8000% immediately after the first cycle (Figure 5d). The hysteresis loop became nearly negligible. The ΔU values of the second cycle of all the nanocomposite hydrogels were extremely small (Figure 5e). After storage at 25 °C for 5 days (or 80 °C for 20 h), the residual strains of tested M_5A and $M_{10}A$ hydrogels were recovered completely (Figure 6). A subsequent third tensile loading–unloading test of the restored hydrogels with ε_m 8000% presented a loop identical to that of the original hydrogel (Figure 5d), indicating a full recovery of the PAAm/MMT adsorption to the original level. Moreover, the ultimate tensile tests were performed on the tested and recovered hydrogels. Tensile stress–strain curves of recovered M_5A and $M_{10}A$ samples were very close to those for the as-prepared hydrogels (Figure 5f).

The effect of clay contents on the recovery of the nanocomposite hydrogels has been systematically investigated by tracking the residual strain evolution over time at 25 and at 80 °C (Figure 6). With a low clay content ($n \leq 10$), the residual strain was fully recovered to the original level. With a high clay content ($n > 10$), unrecoverable strains were left after restored for a long time. These unrecoverable strains were attributed to the alignment and stacking of clay platelets in hydrogels under

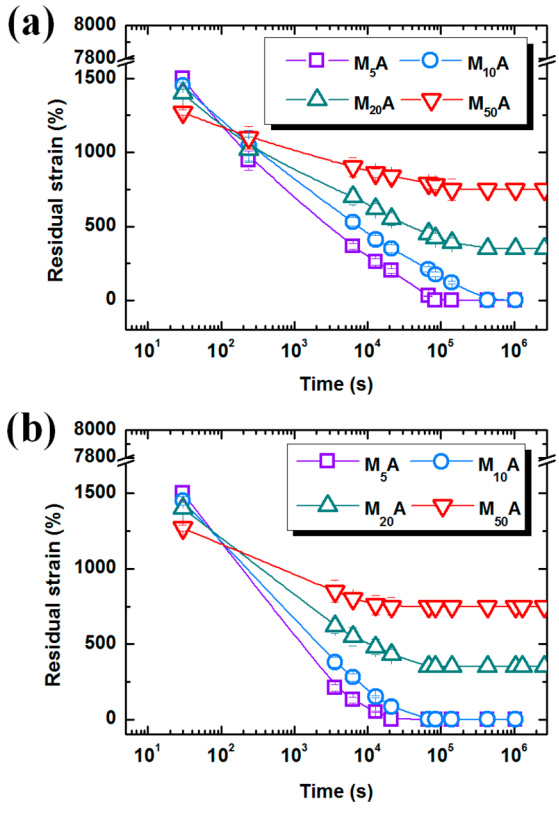

Figure 6. Length recovery over time of M_nA hydrogels after unloading from 8000% strain and then restored at 25 °C (a) and 80 °C (b).

DOI: 10.1021/acsami.5b00704
ACS Appl. Mater. Interfaces 2015, 7, 5029–5037

large deformation, particularly with high clay contents.[53] In the case of M_nA hydrogels, the MMT nanoplatelets are likely oriented along the stretching direction at very high strains. It would be very difficult to readjust their orientation due to the high aspect ratio. As a result, hydrogels with $n > 10$ failed to recover to the original length and showed high residual strains (Figure 6). On the other hand, the aligned clay nanoplatelets may show less rotation and/or deformation upon stretching,[52] and thus allow for less energy dissipation in comparison to those in as-prepared hydrogels. The recovered M_nA hydrogels showed a plateau ΔU value of about 2.5 MJ m^{-3} with n from 20 to 50 (Figure 5c).

Self-Healing of PAAm/MMT Nanocomposite Hydrogels. Short rods of M_nA hydrogels, when put together, could spontaneously adhere at room temperature. However, this adhesion is weak and easily disrupts at the interface. To achieve full healing, the preliminarily jointed rods were slowly dried to a water content of about 10 wt %. Subsequently, these hydrogels were reswollen at room temperature to its original water content. As a result, the rods were merged into a single bar. This self-healing procedure could be applied to hydrogels with identical or different clay contents. The healed hydrogels are able to endure bending (Figure 7a) and high stretching (Figure 7b). During stretching, segments with different clay contents yielded and necked separately, due to the redistribution of stress among the segments with different moduli. More photographs of stretched self-healed hydrogel rods are shown in Figure S5 (Supporting Information). None of these self-healed hydrogels fractured at the interface, which indicates that the healing interface was no longer the weak point.

Figure 7c displays the representative tensile stress–strain curves of self-healed M_5A, $M_{10}A$, $M_{20}A$, and $M_{50}A$ hydrogels, in comparison to their as-prepared counterparts with the same water contents. The modulus, yielding strength, and fracture strength are all higher for the self-healed gels than the latter (Figure 7c, Table S1, Supporting Information). Besides, the fracture strains of self-healed hydrogels are very close to the as-prepared gels. These results indicate a complete healing of the cut segments.

We emphasize that full self-healing was only achieved through the drying–reswelling procedure, which is easy and reproducible under mild conditions without using any healing agents. During this process, the preliminary contact of the cut segments is critical for the diffusion of polymers across the interface. Subsequent drying drives the diffused polymers to closely contact the clay platelets, which is vital to establish strong PAAm/MMT adhesion. Similar drying process in nanocomposite hydrogels has been suggested to strengthen the loose and weak chain/clay contacts in the as-prepared hydrogel and create additional cross-links in highly concentrated state.[15] Thus, the final reswelling gradually hydrated the newly established network and generated intact cross-linked structures.

Otherwise, maintenance of preliminarily contacted hydrogel rods at room temperature or elevated temperatures failed to achieve full healing. Maintenance at room temperature for 7 days resulted in hydrogels with highly reduced fracture strain (<1800%) and strength (<25 kPa, Figure 8a). Further extending the healing time did not improve the healing level. For example, restoration at 80 °C for 7 days improved the fracture strength and strain (Figure 8b), but these values were far below the levels for the as-prepared hydrogels.

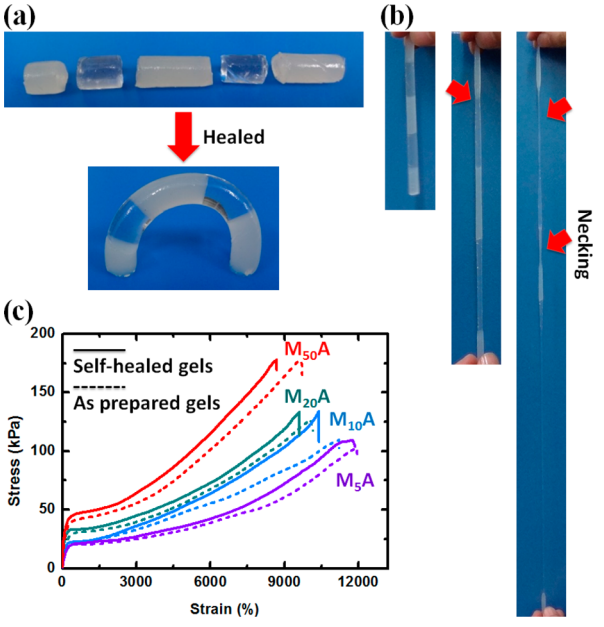

Figure 7. (a) Self-healing of M_5A and $M_{20}A$ rods. (b) Ultrastretching of the healed hydrogels shows separate necking of segments with different clay contents. (c) Representative ultimate tensile stress–strain curves of self-healed M_5A, $M_{10}A$, $M_{20}A$, and $M_{50}A$ hydrogels (solid lines), in comparison to the as-prepared counterparts (dashed lines).

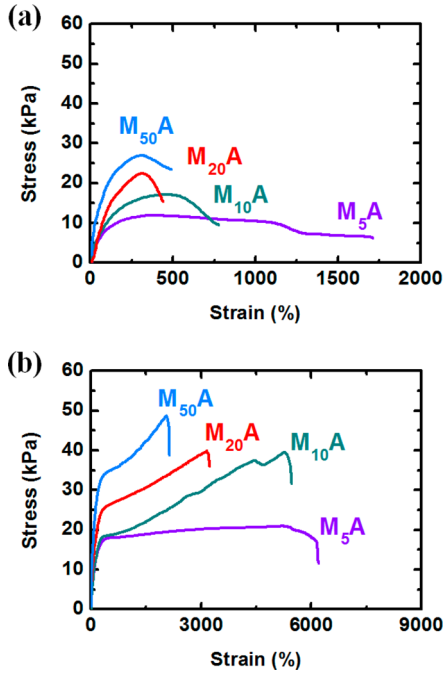

Figure 8. Tensile stress–strain curves of M_nA hydrogels healed by maintenance of the preliminarily contacted hydrogel rods at 25 °C (a) and 80 °C (b) for 7 days.

CONCLUSION

Nanocomposite hydrogels composed of exfoliated sodium montmorillonite showed unprecedented yielding, necking, and a fracture strain up to 11 800% and a fracture energy up to 10.1 MJ m^{-3}. Such hydrogels were synthesized by in situ polymerization of acrylamide with the presence of exfoliated MMT

DOI: 10.1021/acsami.5b00704
ACS Appl. Mater. Interfaces 2015, 7, 5029–5037

platelets that have high aspect ratio. The strong polymer/clay interactions are suggested to account for the unexpected mechanical strength and toughness. Moreover, based on the reversible desorption/readsorption of polymer chains, these nanocomposite hydrogels exhibited capabilities to fully recover at room temperature after stretching or self-heal through a drying−reswelling procedure. We believe these self-healable and super tough hydrogels will stimulate broad research interests on novel hydrogels for potential applications in artificial muscle, actuators, and functional thin films and coatings.

■ ASSOCIATED CONTENT

Supporting Information

TEM images of M_5A hydrogels, photographs of $M_{20}A$ hydrogels swelled in deionized water and dissolved in urea solution, more cyclic tensile curves with stepwise increasing strain, loading−unloading curves of $MBAA_{0.1}A$ hydrogel, photographs of healed hydrogels, and table of mechanical properties of healed hydrogels. This material is available free of charge via the Internet at http://pubs.acs.org.

■ AUTHOR INFORMATION

Corresponding Author

*J. Fu. E-mail: fujun@nimte.ac.cn.

Funding

This project was supported by the Hundred Talents Program of the Chinese Academy of Sciences (J.F.) and the Zhejiang Natural Science Foundation of China (LR13B040001).

Notes

The authors declare no competing financial interest.

■ REFERENCES

(1) Cui, J.; del Campo, A. Multivalent H-bonds for Self-Healing Hydrogels. *Chem. Commun.* **2012**, *48*, 9302−9304.
(2) Phadke, A.; Zhang, C.; Arman, B.; Hsu, C.-C.; Mashelkar, R. A.; Lele, A. K.; Tauber, M. J.; Arya, G.; Varghese, S. Rapid Self-Healing Hydrogels. *Proc. Natl. Acad. Sci. U. S. A.* **2012**, *109*, 4383−4388.
(3) Zhang, H.; Xia, H.; Zhao, Y. Poly(vinyl alcohol) Hydrogel Can Autonomously Self-Heal. *ACS Macro Lett.* **2012**, *1*, 1233−1236.
(4) Akay, G.; Hassan-Raeisi, A.; Tuncaboylu, D. C.; Orakdogen, N.; Abdurrahmanoglu, S.; Oppermann, W.; Okay, O. Self-Healing Hydrogels Formed in Catanionic Surfactant Solutions. *Soft Matter* **2013**, *9*, 2254−2261.
(5) Tuncaboylu, D. C.; Argun, A.; Sahin, M.; Sari, M.; Okay, O. Structure Optimization of Self-Healing Hydrogels Formed via Hydrophobic Interactions. *Polymer* **2012**, *53*, 5513−5522.
(6) Kakuta, T.; Takashima, Y.; Nakahata, M.; Otsubo, M.; Yamaguchi, H.; Harada, A. Preorganized Hydrogel: Self-Healing Properties of Supramolecular Hydrogels Formed by Polymerization of Host-Guest Monomers that Contain Cyclodextrins and Hydrophobic Guest Groups. *Adv. Mater.* **2013**, *25*, 2849−2853.
(7) Nakahata, M.; Takashima, Y.; Yamaguchi, H.; Harada, A. Redox-Responsive Self-Healing Materials Formed from Host-Guest Polymers. *Nat. Commun.* **2011**, *2*, 511−512.
(8) Zhang, M.; Xu, D.; Yan, X.; Chen, J.; Dong, S.; Zheng, B.; Huang, F. Self-Healing Supramolecular Gels Formed by Crown Ether based Host-Guest Interactions. *Angew. Chem., Int. Ed.* **2012**, *51*, 7011−7015.
(9) Yang, J.; Deng, L.-H.; Han, C.-R.; Duan, J.-F.; Ma, M.-G.; Zhang, X.-M.; Xu, F.; Sun, R.-C. Synthetic and Viscoelastic Behaviors of Silica Nanoparticle Reinforced Poly(acrylamide) Core-Shell Nanocomposite Hydrogels. *Soft Matter* **2013**, *9*, 1220−1230.
(10) Zhao, X. Multi-scale Multi-mechanism Design of Tough Hydrogels: Building Dissipation into Stretchy Networks. *Soft Matter* **2014**, *10*, 672−687.
(11) Sun, J.-Y.; Zhao, X.; Illeperuma, W. R. K.; Chaudhuri, O.; Oh, K. H.; Mooney, D. J.; Vlassak, J. J.; Suo, Z. Highly Stretchable and Tough Hydrogels. *Nature* **2012**, *489*, 133−136.
(12) Rose, S.; Prevoteau, A.; Elziere, P.; Hourdet, D.; Marcellan, A.; Leibler, L. Nanoparticle Solutions as Adhesives for Gels and Biological Tissues. *Nature* **2014**, *505*, 382−385.
(13) Rose, S. V.; Dizeux, A.; Narita, T.; Hourdet, D.; Marcellan, A. Time Dependence of Dissipative and Recovery Processes in Nano-hybrid Hydrogels. *Macromolecules* **2013**, *46*, 4095−4104.
(14) Wu, Z. L.; Kurokawa, T.; Gong, J. P. Novel Developed Systems and Techniques Based on Double-Network Principle. *Bull. Chem. Soc. Jpn.* **2011**, *84*, 1295−1311.
(15) Haraguchi, K.; Li, H.-J.; Ren, H.-Y.; Zhu, M. Modification of Nancomposite Gels by Irreversible Rearrangement of Polymer/Clay Network Structure through Drying. *Macromolecules* **2010**, *43*, 9848−9853.
(16) Haraguchi, K.; Takehisa, T. Nanocomposite Hydrogels: A Unique Organic-Inorganic Network Structure with Extraordinary Mechanical, Optical, and Swelling/De-swelling Properties. *Adv. Mater.* **2002**, *14*, 1120−1124.
(17) Haraguchi, K.; Farnworth, R.; Ohbayashi, A.; Takehisa, T. Compositional Effects on Mechanical Properties of Nanocomposite Hydrogels Composed of Poly(N,N-dimethylacrylamide) and Clay. *Macromolecules* **2003**, *36*, 5732−5741.
(18) Haraguchi, K. Synthesis and Properties of Soft Nanocomposite Materials with Novel Organic/Inorganic Network Structures. *Polym. J.* **2011**, *43*, 223−241.
(19) Xiong, L.; Hu, X.; Liu, X.; Tong, Z. Network Chain Density and Relaxation of *in Situ* Synthesized Polyacrylamide/Hectorite Clay Nanocomposite Hydrogels with Ultrahigh Tensibility. *Polymer* **2008**, *49*, 5064−5071.
(20) Liu, R.; Liang, S.; Tang, X.-Z.; Yan, D.; Li, X.; Yu, Z.-Z. Tough and Highly Stretchable Graphene Oxide/Polyacrylamide Nanocomposite Hydrogels. *J. Mater. Chem.* **2012**, *22*, 14160−14167.
(21) Hu, Z.; Chen, G. Novel Nanocomposite Hydrogels Consisting of Layered Double Hydroxide with Ultrahigh Tensibility and Hierarchical Porous Structure at Low Inorganic Content. *Adv. Mater.* **2014**, *26*, 5950−5956.
(22) Haraguchi, K.; Uyama, K.; Tanimoto, H. Self-Healing in Nanocomposite Hydrogels. *Macromol. Rapid Commun.* **2011**, *32*, 1253−1258.
(23) Liu, J.; Song, G.; He, C.; Wang, H. Self-Healing in Tough Graphene Oxide Composite Hydrogels. *Macromol. Rapid Commun.* **2013**, *34*, 1002−1007.
(24) Podsiadlo, P.; Kaushik, A. K.; Arruda, E. M.; Waas, A. M.; Shim, B. S.; Xu, J.; Nandivada, H.; Pumplin, B. G.; Lahann, J.; Ramamoorthy, A.; Kotov, N. A. Ultrastrong and Stiff Layered Polymer Nanocomposites. *Science* **2007**, *318*, 80−83.
(25) Kulshrestha, P.; Giese, R. F.; Aga, D. S. Investigating the Molecular Interactions of Oxytetracycline in Clay and Organic Matter: Insights on Factors Affecting Its Mobility in Soil. *Environ. Sci. Technol.* **2004**, *38*, 4097−4105.
(26) Biasci, L.; Aglietto, M.; Ruggeri, G. Functionalization of Montmorillonite by Acrylamide Polymers Containing Side-Chain Ammonium Cations. *Polym. Adv. Technol.* **1995**, *6*, 662−670.
(27) Chen, P.; Zhang, L. Interaction and Properties of Highly Exfoliated Soy Protein/Montmorillonite Nanocomposites. *Biomacromolecules* **2006**, *7*, 1700−1706.
(28) Heinz, H.; Koerner, H.; Anderson, K. L.; Vaia, R. A.; Farmer, B. Force Field for Mica-Type Silicates and Dynamics of Octadecylammonium Chains Grafted to Montmorillonite. *Chem. Mater.* **2005**, *17*, 5658−5669.
(29) Dashman, T.; Stotzky, G. Adsorption and Binding of Amino Acids on Homoionic Montmorillonite and Kaolinite. *Soil Biol. Biochem.* **1982**, *14*, 447−456.
(30) Fiorito, T. M.; Icoz, I.; Stotzky, G. Adsorption and Binding of the Transgenic Plant Proteins, Human Serum Albumin, β-Glucuronidase, and Cry3Bb1, on Montmorillonite and Kaolinite: Microbial Utilization

DOI: 10.1021/acsami.5b00704
ACS Appl. Mater. Interfaces 2015, 7, 5029−5037

and Enzymatic Activity of Free and Clay-Bound Proteins. *Appl. Clay Sci.* **2008**, *39*, 142−150.
(31) Yao, H. B.; Tan, Z. H.; Fang, H. Y.; Yu, S. H. Artificial Nacre-like Bionanocomposite Films from the Self-Assembly of Chitosan-Montmorillonite Hybrid Building Blocks. *Angew. Chem., Int. Ed.* **2010**, *49*, 10127−10131.
(32) Wang, L.; Zhang, J.; Wang, A. Removal of Methylene Blue from Aqueous Solution Using Chitosan-*g*-Poly(acrylic acid)/Montmorillonite Superadsorbent Nanocomposite. *Colloids Surf., A* **2008**, *322*, 47−53.
(33) Viseras, C.; Cerezo, P.; Sanchez, R.; Salcedo, I.; Aguzzi, C. Current Challenges in Clay Minerals for Drug Delivery. *Appl. Clay Sci.* **2010**, *48*, 291−295.
(34) Guilherme, M. R.; Fajardo, A. R.; Moia, T. A.; Kunita, M. H.; Gonçalves, M. d. C.; Rubira, A. F.; Tambourgi, E. B. Porous Nanocomposite Hydrogel of Vinyled Montmorillonite-Crosslinked Maltodextrin-co-Dimethylacrylamide as a Highly Stable Polymer Carrier for Controlled Release Systems. *Eur. Polym. J.* **2010**, *46*, 1465−1474.
(35) Klute, A. *Methods of Soil Analysis. Part 1. Physical and Mineralogical Methods*; American Society of Agronomy, Inc.: Madision, WI, 1986.
(36) Nishino, T.; Hayashi, N.; Bui, P. T. Direct Measurement of Electron Transfer through a Hydrogen Bond between Single Molecules. *J. Am. Chem. Soc.* **2013**, *135*, 4592−4595.
(37) Zhang, Y.; Li, Y.; Liu, W. Dipole-Dipole and H-Bonding Interactions Significantly Enhance the Multifaceted Mechanical Properties of Thermoresponsive Shape Memory Hydrogels. *Adv. Funct. Mater.* **2015**, *25*, 471−480.
(38) Liu, D.; Yuan, P.; Liu, H.; Cai, J.; Tan, D.; He, H.; Zhu, J.; Chen, T. Quantitative Characterization of the Solid Acidity of Montmorillonite Using Combined FTIR and TPD Based on the NH_3 Adsorption System. *Appl. Clay Sci.* **2013**, *80*, 407−412.
(39) Okay, O.; Oppermann, W. Polyacrylamide-Clay Nanocomposite Hydrogels: Rheological and Light Scattering Characterization. *Macromolecules* **2007**, *40*, 3378−3387.
(40) Shibayama, M.; Karino, T.; Miyazaki, S.; Okabe, S.; Takehisa, T.; Haraguchi, K. Small-Angle Neutron Scattering Study on Uniaxially Stretched Poly(N-isopropylacrylamide)-Clay Nanocomposite Gels. *Macromolecules* **2005**, *38*, 10772−10781.
(41) Song, G.; Zhang, L.; He, C.; Fang, D.-C.; Whitten, P. G.; Wang, H. Facile Fabrication of Tough Hydrogels Physically Cross-Linked by Strong Cooperative Hydrogen Bonding. *Macromolecules* **2013**, *46*, 7423−7435.
(42) Sperling, L. H. *Introduction to Physical Polymer Science*; John Wiley & Sons, Inc.: Hoboken, NJ, 2005.
(43) Kamata, H.; Akagi, Y.; Kayasuga-Kariya, Y.; Chung, U.-i.; Sakai, T. "Nonswellable" Hydrogel Without Mechanical Hysteresis. *Science* **2014**, *343*, 873−875.
(44) Naficy, S.; Spinks, G. M.; Wallace, G. G. Thin, Tough, pH-Sensitive Hydrogel Films with Rapid Load Recovery. *ACS Appl. Mater. Interfaces* **2014**, *6*, 4109−4114.
(45) Khanlari, A.; Detamore, M. S.; Gehrke, S. H. Increasing Cross-Linking Efficiency of Methacrylated Chondroitin Sulfate Hydrogels by Copolymerization with Oligo (Ethylene Glycol) Diacrylates. *Macromolecules* **2013**, *46*, 9609−9617.
(46) Na, Y. H.; Tanaka, Y.; Kawauchi, Y.; Furukawa, H.; Sumiyoshi, T.; Gong, J. P.; Osada, Y. Necking Phenomenon of Double-Network Gels. *Macromolecules* **2006**, *39*, 4641−4645.
(47) Haraguchi, K.; Ebato, M.; Takehisa, T. Polymer−Clay Nanocomposites Exhibiting Abnormal Necking Phenomena Accompanied by Extremely Large Reversible Elongations and Excellent Transparency. *Adv. Mater.* **2006**, *18*, 2250−2254.
(48) Zhu, M. F.; Liu, Y.; Sun, B.; Zhang, W.; Liu, X. L.; Yu, H.; Zhang, Y.; Kuckling, D.; Adler, H. J. P. A Novel Highly Resilient Nanocomposite Hydrogel with Low Hysteresis and Ultrahigh Elongation. *Macromol. Rapid Commun.* **2006**, *27*, 1023−1028.
(49) Nakajima, T.; Kurokawa, T.; Ahmed, S.; Wu, W.-l.; Gong, J. P. Characterization of Internal Fracture Process of Double Network Hydrogels under Uniaxial Elongation. *Soft Matter* **2013**, *9*, 1955−1966.
(50) Gong, J. P. Why Are Double Network Hydrogels so Tough? *Soft Matter* **2010**, *6*, 2583−2590.
(51) Webber, R. E.; Creton, C.; Brown, H. R.; Gong, J. P. Large Strain Hysteresis and Mullins Effect of Tough Double-Network Hydrogels. *Macromolecules* **2007**, *40*, 2919−2927.
(52) Lian, C.; Lin, Z.; Wang, T.; Sun, W.; Liu, X.; Tong, Z. Self-Reinforcement of PNIPAm-Laponite Nanocomposite Gels Investigated by Atom Force Microscopy Nanoindentation. *Macromolecules* **2012**, *45*, 7220−7227.
(53) Haraguchi, K.; Li, H. J. Mechanical Properties and Structure of Polymer-Clay Nanocomposite Gels with High Clay Content. *Macromolecules* **2006**, *39*, 1898−1905.

DOI: 10.1021/acsami.5b00704
ACS Appl. Mater. Interfaces 2015, 7, 5029−5037